scientific reports

OPEN

Experimental analysis of sequential water alternating CO₂ gas injection for enhancing oil recovery in X-field sandstone reservoir of Cambay basin

Ashutosh Rawat[1,3], Bhaskarjyoti Khanikar[2,3], Abhishek Kumar Samanta[2], Patrick Nguessan[2,3], Bhavesh Mehta[2,3], Anirbid Sircar[2], Bhawanisingh Desai[2], Achinta Bera[2,3] & Namrata Bist[2,3 ✉]

This study evaluates the oil recovery potential of sandstone reservoirs through sequential water-alternating CO₂ gas injection. Experimental work focuses on optimizing injection patterns, including alternating CO₂ and water cycles, to assess their impact on enhanced oil recovery (EOR). Analytical methods performed before detailed analyses include Fourier Transform Infrared (FTIR) Spectroscopy and X-ray diffraction (XRD) on the crude oil and core samples from the same field of Cambay Basin. FTIR analysis revealed a dominance of long-chain aliphatic hydrocarbons, suggesting favorable interactions with CO₂ for viscosity reduction and oil swelling. XRD revealed quartz-dominant cores with subordinate feldspar that control fluid permeability and chemical interactiveness. Sequential Water-Alternating-Gas (WAG) injection improved sweep efficiency by minimizing gas channeling and maximizing CO₂-oil contact. Soak periods conducted during injection enhance some miscibility effects with addition of extra oil mobility. High permeability cores experienced early gas breakthroughs, while low permeability delayed gas movement, achieving better recovery. Reservoir heterogeneities and water-shielding effects were critical challenges, underscoring the role of petrophysical properties in recovery performance. The results demonstrate that CO₂ WAG injection in sandstone reservoirs significantly enhances crude oil recovery by improving oil displacement efficiency. The presented work emphasizes the parameters porosity, permeability, and oil saturation as prerequisites for the process. Collected sandstone core samples show that variations in these properties influence the effectiveness of CO₂ WAG injection showing the resultant oil recovery increase by 20–25% after secondary brine injection. The integration of advanced characterization and strategic injection patterns establishes a foundation for optimizing CO₂ EOR in mature fields.

Keywords WAG injection, CO₂ flooding, Gas channeling, Sweep efficiency, Oil recovery factor

The main anthropogenic causes of climate change exist in the emissions of greenhouse gases, especially CO_2 which in turn enhanced the world's average atmospheric temperature and had climbed by approximately 2.5 °C by 2020[1,2]. In the oil and gas industry where the emission of CO_2 is high, CO_2 EOR ushers in a balance since the captured CO_2 is injected mainly into primarily deficit reservoirs thereby cutting total greenhouse gas emissions. Carbon capture utilization & storage technology represents a significant breakthrough in tackling this issue. Among the various projects, CO_2-EOR is a critical method for CO_2 usage and sequestration. It can boost the oil recovery factor by 8–15%, with 2.4–3 tons of CO_2 required to inject $1\,m^3$ of extra oil[3]. The process relies on the solubility of CO_2 in the oil, reducing its viscosity due to swelling, and enhancing its flow towards the production wells. Moreover, there is the ability of CO_2 to react with rock grains which changes the wettability and increases the oil displacement.

[1]Oil and Natural Gas Corporation Limited, Mumbai 400051, India. [2]Department of Petroleum Engineering, School of Energy Technology, Pandit Deendayal Energy University, Gandhinagar 382426, India. [3]Drilling, Cementing, and Stimulation Research Center, Pandit Deendayal Energy University, Gandhinagar 382426, India. ✉email: Namrata.Bist@spt.pdpu.ac.in

Oil bypassing, fluid front instability and an early breakthrough in the swept area of a reservoir are all consequences of low microscopic sweep efficiency of gas injection operations owing to the low viscosity of gas and large density difference between the gas and crude oil reservoir[4,5]. Thus, CO_2-WAG (Water Alternating Gas) injection is a proven CO_2-EOR technology, which has worked effectively in all applications, ranging from pore- to field-scale. By lowering its relative permeability and partially diverting the gas by filling up the flow channels, which CO_2 invaded earlier, WAG injection can effectively minimize the mobility of CO_2 and increase oil recovery and macroscopic sweep efficiency[6]. Figure 1 depicts the relative front flow contrast of CO_2 flooding and WAG injection in the simplest form.

For crude oil to become miscible, the CO_2 would need to be supercritical – exhibiting both gaseous and liquid-like behaviours and penetrate further into the oil[7]. Miscible CO_2 flooding is only viable through rupturing of Minimum Miscibility Pressure (MMP): pressure through which CO_2 and oil mix completely i.e. it works as a single phase[8]. Between this range, the oil displacement efficiency is at its maximum high since interfacial tension among the two phases is nearly zero and MMP emerges as a key parameter that dictates the performance and optimization of CO_2 flooding operations[9].

In CO_2 immiscible flooding, the interfacial tension (IFT) between residual oil and CO_2 is non-zero, and this affects the process efficiency[10]. Waterflooding is the most applied secondary recovery process, preceded by tertiary gas injection. High water saturation causes a water shielding effect that prevents the injected solvent from effectively contacting the remained oil, especially in water-wet reservoirs[11]. This means that the injected gas would have varying contact and miscibility modes, drastically reducing its displacement efficiency[12,13]. High water saturation and its influence in controlling the CO_2 flooding performance of mature oilfields is emphasized in this study.

Such continuous CO_2 injection may cause coalescence of viscously trapped oil in the CO_2 phase with resultant low sweep and low oil recovery, reducing CO_2 storage efficiency for which WAG is suggested[14,15]. The process can be an effective means of augmentation of oil recovery in sandstone reservoirs by utilizing a specified injected pore volume of CO_2 and water for alternating injection of CO_2-EOR. Reducing the difference in mobility between the resident oil and injected CO_2 significantly increases sweep efficiency along with contact between them, which is reasonable in the case of heterogeneous sandstone reservoirs. Besides, as in the sole injection of CO_2, water and CO_2 alternate injection maintains the reservoir pressure at a desired rate and pressure that does not fracture the reservoir rock[16,17].

The general CO_2 retention and recovery efficiency within the reservoir is greatly influenced by the size of the CO_2 and water slug and the soaking time between injections[18]. CO_2 EOR is an essential part of the cleaner energy transition because it guarantees increased oil recovery, efficient greenhouse gas mitigation, and economic viability when these elements are properly optimized[19]. To begin with, higher oil production is directly proportional to higher CO_2 injection rates. The injection rate has to be established nominally based on economic considerations in an effort to avoid formation damage and early breakthrough[20]. Similar to the huff-and-puff process of thermal EOR, the optimum soak period in CO_2 WAG injection is desirable because it permits the injected CO_2 to penetrate into the oil and lower its viscosity and enhance its mobility. Through enhanced oil swelling and dissolution over the duration of soak, the CO_2 acts on the reservoir fluids to increase the displacement efficiency in later phases of production[21].

Residual oil becomes isolated from encountering gas contact because of the injected water. A high water-to-oil interface tension results in difficult to remove trapped oil, which leads to reduced microscopic sweep efficiency[22]. Gas chambers form because of gravity segregation in reservoirs with high vertical permeability, which results in early formation of gas breakthroughs. The WAG process operation efficiency declines due to this phenomenon, which also adversely affects its volumetric sweep performance[23]. Natural gravity segregation of oil and gas causes early gas breakthroughs because high vertical permeability allows gas to override the oil as
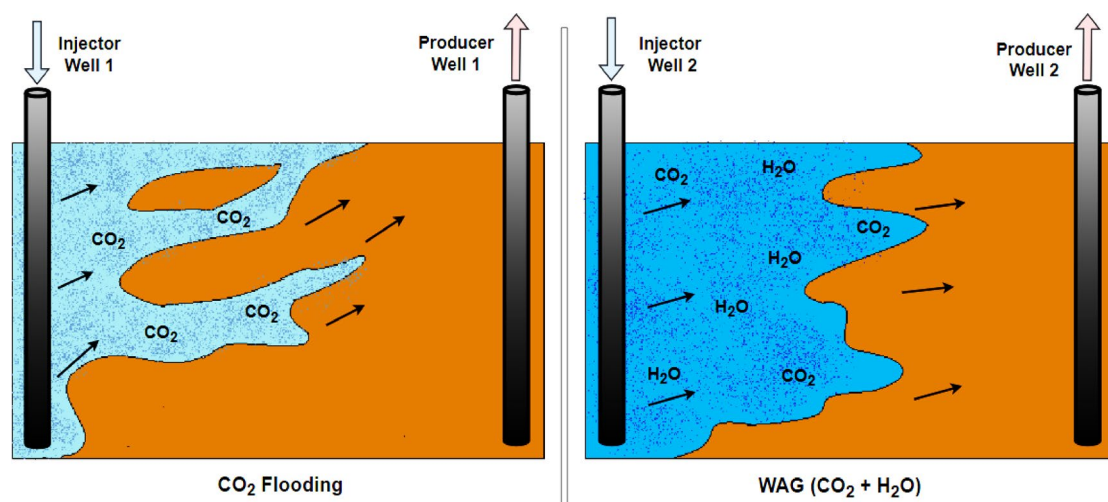

Fig. 1. Simplified diagram comparing injected fluid front flow between CO_2 flooding and WAG injection.

it flows through the reservoir. The WAG process becomes less effective due to this occurrence, which decreases the recovery of swept reservoir volumes[24].

This study presents a compatible work by systematically investigating the effects of sequential CO_2-WAG injection with controlled soak periods and variable injection rates customised to X-field sandstone cores in the Cambay Basin to minimise drawbacks from WAG injection. It combines optimal slug volumes, soak periods, and injection sequences to achieve maximum oil recovery, as opposed to traditional continuous CO_2 injection, which is defined by poor sweep efficiency and early breakthrough. The study presents some data about rock-fluid interactions by combining petrophysical characteristics and geochemical investigations, such as FTIR and XRD. A good understanding of the reservoir and fluid parameters is needed to analyze the oil recovery data and optimize the injection technique, and for that reason, these determinations were undertaken.

Materials and methods

Materials
Three core samples were collected from X-field of Cambay Basin for Laboratory research basis, coded as 'BB,' 'B' and 'K.' The samples were first cleaned thoroughly to remove any residual fluids, contaminants, or loose particles, typically using solvents and drying methods. This was followed by crushing a small portion of the cores into fine powders to achieve the required particle size for XRD analysis. The other 95% of the core was trimmed and smoothened, giving a certain length and diameter for measuring porosity and permeability and fitting in the core holder for further flooding. An efficient amount of crude oil samples was collected from a particular well of that field for its characterization to be feasible for further CO_2 injection with the prescribed cores. A brine solution with a salinity of 15,450 ppm (15.43 g/L) was prepared to replicate the salinity of the oil field reservoir water and was used during the injection process.

Methods
Crude oil characterization
Characterization of crude oil is essential for determining its suitability for CO_2 EOR applications. The crude oil collected from a specific well of X-field in Cambay basin has an API gravity of 24° measured using the ASTM D1298 method[25] indicating medium crude oil, which shows the potential for CO_2-EOR. A highly effective viscosity of 87 cP was calculated at a higher shear rate at an elevated temperature of 80 °C using an Anton Paar Rheometer. Water content was determined to be 5.5% by using the ASTM D4007 method[26]. By using UOP 46/64 method[27] significant wax content of 12.2% and asphaltene content of 2.5% was found. With the ASTM D97 method[28], a low pour point at 12 °C was measured. Based on the above parameters, it can be said that crude oil can cause some potential issues with deposition and flow assurance in wellbores. But the combination of CO_2 and water can mitigate those by altering the oil's rheological properties and maintaining flow in the reservoir, and also in wellbore conditions[29]. A simplified flow chart was shown in Fig. 2, which shows the requirements for characterizing crude oil.

FTIR analysis was conducted before Water Alternating CO_2 Gas injection, which was beneficial as it provides a baseline chemical fingerprint of crude oil, particularly identifying functional groups in asphaltenes and waxes. This helps predict the potential for precipitation or deposition issues, but when CO_2 and water are introduced[29,30].

Based on the FTIR analysis results, numerous information can be found about the composition and characteristic functional groups present in the collected crude oil, mainly in the context of wax and asphaltene deposits. The strong peaks at 2952 cm⁻¹ (symmetric CH₃ stretching), 2925 cm⁻¹ (asymmetric CH₂ stretching),
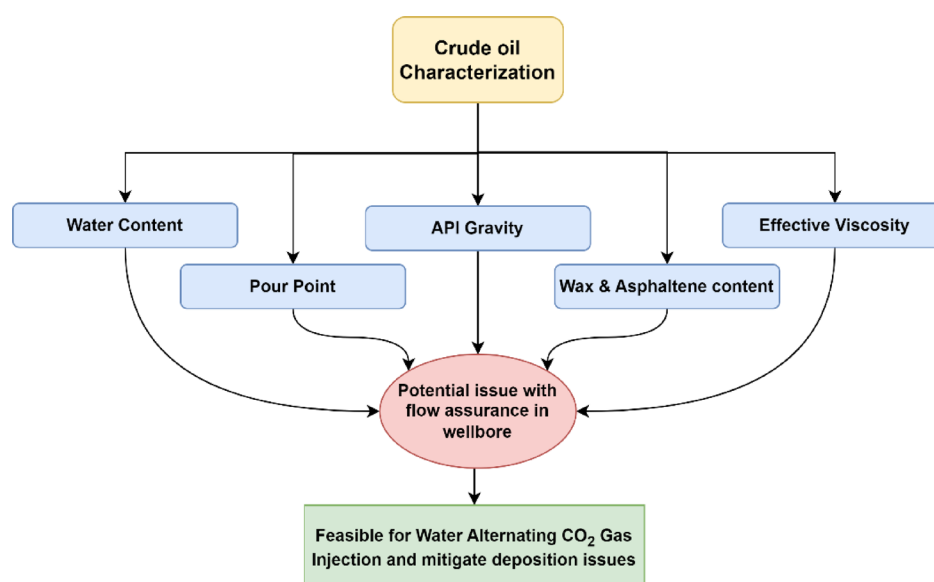

Fig. 2. Flow chart representing the importance of crude oil characterization.

Wavenumber (cm⁻¹)	Vibration Type	Intensity
2952	Symmetric CH_3 stretching	Strong
2925	Asymmetric CH_2 stretching	Strong
2853	Symmetric CH_2 stretching	Strong
1458	CH_2 scissoring or CH_3 deformation	Medium
1377	Bending CH_3 (methyl group)	Medium
813	Out-of-plane bending of aromatic rings	Weak
743	Out-of-plane bending of aromatic rings	Weak
721	Rocking CH_2 (in the alkyl side chain of aromatics)	Weak

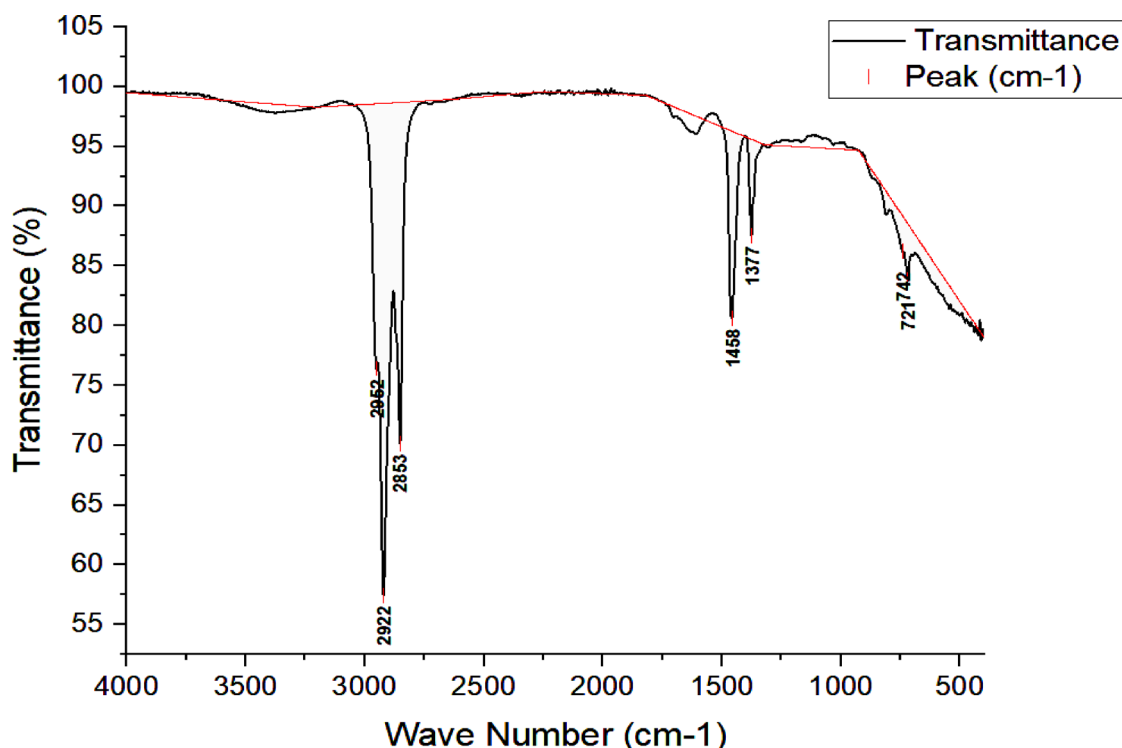**Table 1**. Wave number and associated stretching frequency present in the crude oil.

Fig. 3. FTIR wave spectrum concerning the transmittance of the crude oil sample.

and 2853 cm⁻¹ (symmetric CH_2 stretching) indicate the presence of aliphatic hydrocarbons, showing the dominance of long-chain alkanes typical of crude oil[31]. Peaks at 1458 cm⁻¹ (CH_2 scissoring or CH_3 deformation) and 1377 cm⁻¹ (bending CH_3) indicate alkyl chains in saturated hydrocarbons, providing additional proof. Weak peaks at 813 cm⁻¹ and 743 cm⁻¹, which correspond to out-of-plane bending of aromatic rings, show the presence of aromatic chemicals, but in smaller proportions than aliphatic components. The 721 cm⁻¹ peak implies CH_2 rocking in alkyl side chains attached to aromatic rings, indicating alkyl-substituted aromatic hydrocarbons like alkylbenzenes. Overall, larger aliphatic peaks suggest a greater abundance of aliphatic hydrocarbons (such as paraffins and alkanes), whereas weaker aromatic peaks indicate a lower proportion of aromatic hydrocarbons. The 721 cm⁻¹ signal indicates the presence of long alkyl chains or side chains on aromatic rings, which are typical in waxy or paraffinic crude oils, indicating the sample's complex molecular structure[32]. Table 1 displays the FTIR spectrum analysis of the crude oil sample in tabular format, while Fig. 3 depicts the crude oil sample's wave number versus transmittance, indicating multiple peaks.

The strong CH_2 and CH_3 stretching bands in the FTIR spectrum reveal the existence of numerous functional groups like copious amounts of long-chain aliphatic hydrocarbons[33]. The weaker out-of-plane bending bands also reveal the existence of aromatic chemicals, according to the study. These results determine the molecular complexity of the sample by way of evidence of the presence of both aliphatic and aromatic structures, which can be a significant factor in determining the behavior and reactivity of the oil[34]. They are predominantly long-chain aliphatic hydrocarbons, typical of paraffinic oils. This indicates that by lowering the viscosity and inducing swelling upon injection, these hydrocarbons will have good interaction with CO_2 to improve oil mobility and displacement efficiency. The presence of aromatic hydrocarbons increases the chemical stability of crude oil and affects miscibility of the oil with CO_2 under specific temperature and pressure conditions. Moreover, the

calculated hydrocarbon content and functional groups may affect wettability alteration occurring after WAG injection, especially for water-wet sandstone reservoirs. Through contact angle alteration and enhanced sweep efficiency, such interactions can ultimately enhance the recovery of oil.

Rock characterization

Porosity determination The pore volume (PV) of a core sample, indicative of its porosity, was determined by the water saturation method. The core was first dried at some elevated temperature (70–110 °C) for 24 h to remove any water particles. After drying, its dry weight (W_1) was measured, and its physical dimensions (length and diameter) were recorded to calculate the bulk volume (BV). The core was then saturated in water for 48 h, and its wet weight (W_2) was measured. The PV was calculated as (W_2-W_1)/, where is the density of pure water. Porosity was then determined as PV/BV.

Permeability determination The core flood displacement method has been used to calculate the rock permeability. In a linear core flood experiment, the permeability data were obtained by applying Darcy's law. The study evaluated forward and backwards flow permeabilities using the rubber core sleeve displacement method at sleeve pressures of 300 and 500 psi.

XRD determination The XRD analysis of the three sandstone core samples was conducted to identify their mineralogical composition. The core samples were first finely ground into powder to ensure uniformity. The powdered samples were then placed in the X-ray diffractometer and exposed to X-rays over a 2θ range of 5° to 80°. The diffracted X-rays produced characteristic peaks corresponding to the mineral phases present in the samples. The intensity and position of these peaks were analyzed to identify dominant minerals such as quartz, feldspar, etc.

The XRD plot of the three sandstone core samples in Fig. 4 showed major peaks ranging from 5° to 80°. It revealed that quartz (Sio2) was the major mineral present in all the sandstones, followed by the least intense peaks of feldspar minerals such as illite ($K_{1-1.5}Al_4(Si, Al)8O_{20}(OH)_4$) and albite ($NaAlSi_3O_8$) (white feldspar). Quartz shows high-intensity peaks at 26.6°, and short peaks between 30° to 70° for all three cores, which confirms its abundance in the sandstone matrix. Feldspar showed lower peaks ranging around 20°, indicating the presence of illite and the other peak near 28° of K core represents albite[35,36]. These mineralogical compositions suggest that quartz's strong mechanical properties dominate the core structure, while feldspar may contribute to the chemical interactions during CO_2 flooding[37].
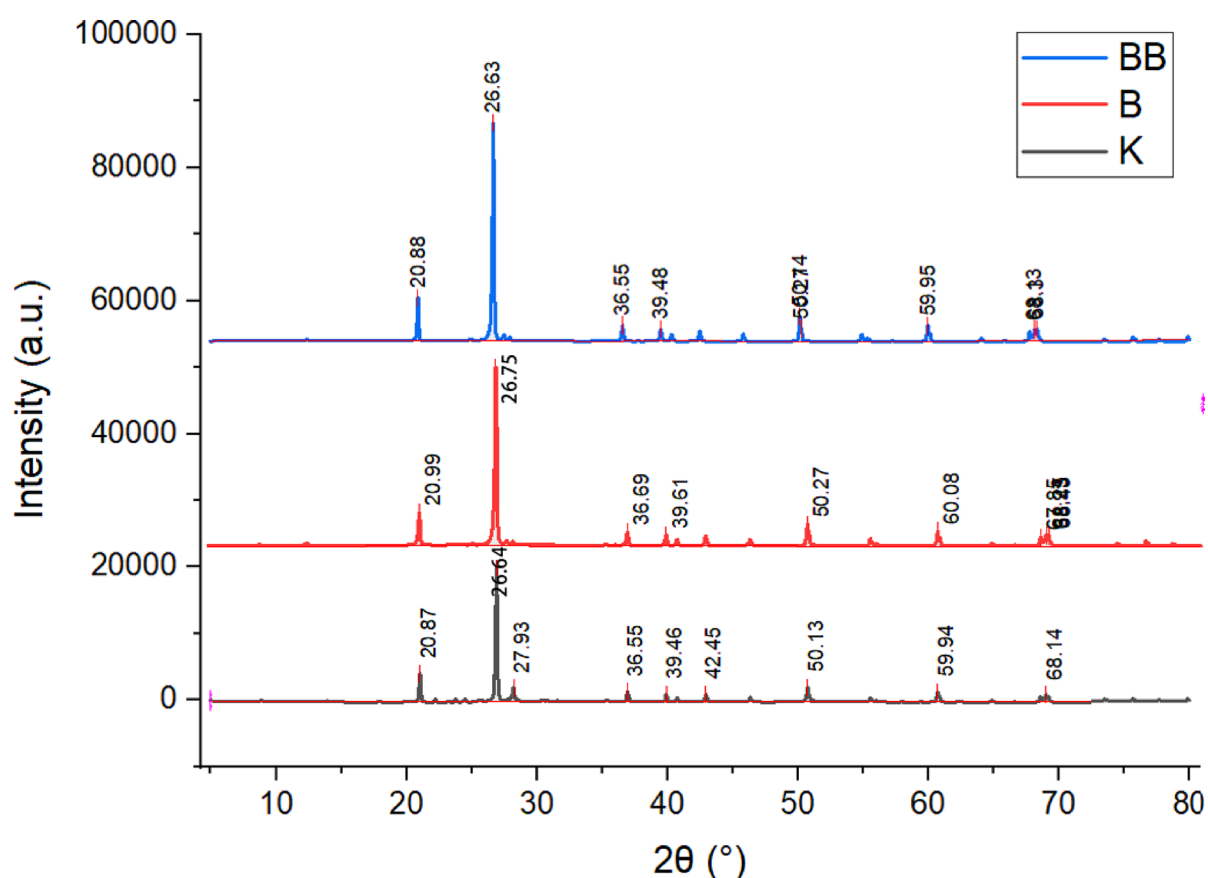

Fig. 4. XRD analysis of three sandstone core samples depicting various peaks.

However, the negligible presence of kaolinite, though minimal, could be detected within the lowest peaks along with quartz, which does not have much potential to reduce permeability and affect sweep efficiency[38]. Overall, the high quartz content provides a stable framework, while feldspar minerals contribute to the chemical reactivity and can influence negligible CO_2 solubility with the core minerals.

MMP calculation based on correlation
The equation applied for MMP correlation was developed by Yellig & Metcalfe[39], which is shown in Eq. 1. This correlation was based on experimental observations to estimate MMP for CO_2-oil systems. It primarily incorporates the oil's API gravity of 24° and reservoir temperature of 176 °F (80 °C) as critical parameters, reflecting their impact on the interaction between CO_2 and crude oil. It assumes that higher API gravity oils and elevated temperatures generally lower the MMP, improving the miscibility potential of CO_2 with oil. The reservoir formation pressure of the X-field zone from where the crude oil has been collected was around 114 kg/cm³ (11.18 MPa)[40,41]. The overall MMP based on the correlation was found to be 31.45 MPa (4560 psi), which is also much higher than the original formation pressure of the reservoir. It is difficult to realize multiple contact miscibility in CO_2 flooding.

$$MMP = \left[-329.558 + \left\{ 7.727 \times \left(\frac{8864.9}{API} \right)^{\frac{1}{1.012}} \times 1.005^T \right\} - \left\{ 4.377 \times \left(\frac{8864.9}{API} \right)^{\frac{1}{1.012}} \right\} \right] \div 145 \quad (1)$$

Research indicates that partial miscibility of CO_2 with oil can contribute to EOR by improving oil displacement efficiency, even when the MMP is not fully achieved. CO_2, under certain conditions, can dissolve partially into crude oil, leading to oil swelling, viscosity reduction, and an increase in mobility, which facilitates oil recovery[42,43].

Experimental setup
The setup for sequential water-alternating CO_2 gas injection was designed to replicate reservoir conditions and evaluate the efficiency of this method, which is shown in Fig. 5. The system starts with a CO_2 cylinder, which supplies the required gas for the flooding experiment. Connected to a pressure gauge, the CO_2 cylinder ensures precise control over the injection pressure. Synthetic brine water and crude oil are stored in specific cylinders, respectively. These fluids are injected into the core holder using a booster (displacement) ISCO pump for bulk fluid transfer and an injection pump for precise control of flow rates.

An essential part of the setup is the triaxial core holder, which holds the rock core sample. To replicate the in-situ stresses of the reservoir environment, it was exposed to confining pressure using an overburden pressure pump while being kept within a hot air oven to preserve reservoir temperature conditions, which are normally approximately 80 °C. An N_2 cylinder was included in the setup to ensure that reservoir conditions were precisely mimicked by maintaining back pressure throughout the experiment. In addition to preventing premature gas breakthroughs during floods and abrupt high-pressure fluctuations that could harm the core holder and other components, back pressure aids in system stabilization.

To saturate the core and provide initial water saturation, brine is injected first in the experimental process, which entails sequential injection. Next, CO_2 is injected to push out the crude oil from the core. Again, water was injected to assist the CO_2 movement, which is illustrated by reciprocal cycles of CO_2 and brine to maximize oil displacement. A soak time of one hour was given after every CO_2 slug injection to have at least some partial dissolving tendency with the oil in the core. The fluids produced in the core holder were led to a three-phase separator, which splits the product into three phases, i.e., water (or emulsion), crude oil, and CO_2. All the phases can be separated individually, for further quantitative and qualitative analysis can be done in the separator.

Part of the apparatus is driven by an air compressor, and a data acquisition and control system continuously collects and stores experimental parameters like temperature, pressure, and flow rate. This entire setup tried to replicate reservoir conditions, and worthwhile information about how efficiently water-alternating CO_2 gas injection works as an EOR method is provided.

Experimental conditions
To allow an accurate simulation of reservoir conditions, several starting conditions were well-defined prior to initiating the flooding process. The X-field crude oil sample was fully characterized to establish its behaviour and characteristics under the experimental setup described in the crude oil analysis section. Table 2 lists the fundamental characteristics of the three little core samples that were taken from full-diameter cores. After a 24-hour vacuum of the sand core samples, high-salinity water was added to start the saturation process at a specific rate of 0.5 ml/min at an experimental pressure of 5.5 MPa.

Similarly, after almost 100% water saturation, drainage process was conducted by flooding the core at an elevated temperature of 80 °C and injecting at a rate of 0.1 ml/min for uniform distribution, leaving residual water saturation. Oil saturation was calculated based on the determined pore volume of the core sample using the saturation method alongside the volume of oil extracted. The original oil in place for each core sample was calculated based on its specific oil saturation and pore volume.

CO_2 gas cylinders (99% pure) were employed to provide the injected gas required for the flooding sequence to facilitate effective oil displacement. Overburden pressure in the range of 800–1000 psi was applied to the core sample using an overburden pressure pump to prevent expansion, shifting, and changes in the pore structure, while also eliminating issues such as non-uniform flow and channelling that could have affected the results. Additionally, nitrogen gas from an N_2 cylinder was used to maintain a back pressure of 300–400 psi, ensuring consistent flow, avoiding phase separation and fluid instability, and preventing early breakthrough or damage to the core and equipment. These preparatory steps were followed to maintain the integrity of the experiment and to obtain reliable data for evaluating the effectiveness of water-alternating CO_2 gas injection.
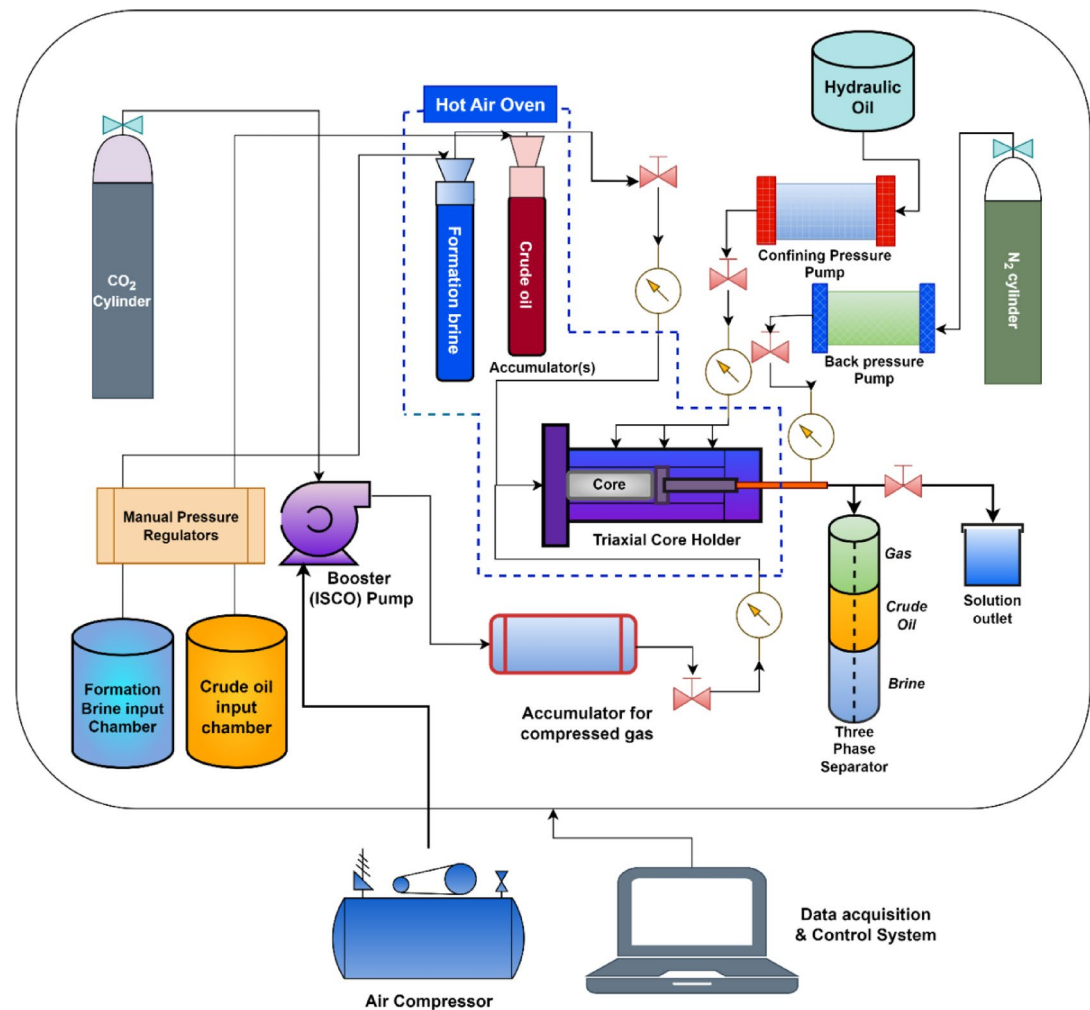
Fig. 5. Schematic Diagram of the Displacement mechanism used for the flooding process.

Core code	Length (cm)	Diameter (cm)	Porosity (%)	Permeability (%)	Pore Volume (cm³)	Oil saturation (%)
BB	12.45	3.8	28.19	285	39.32	75.5
B	12.45	3.8	23.2	190	32.48	71.2
K	12.45	3.8	17.35	116	22.5	63.8

Table 2. Basic parameters of the core samples.

Although it was immiscible flooding of CO_2, as the calculated high MMP was not feasible with the reservoir pressure for miscibility, the process was conducted to evaluate each core oil recovery factor without crude oil being completely miscible with the oil. But a soak time follows, allowing CO_2 to dissolve in oil at least in a small portion with the respective injection pressure, allowing oil swelling and reducing its viscosity. Subsequently, brine water is injected to maintain reservoir pressure and improve displacement. The sequence concludes with a final CO_2 injection to maximize recovery, continuing until production ceases. This method optimizes the synergistic effects of CO_2 and water in enhancing oil recovery.

Result and discussion
Sequential injection pattern
The core flooding experiment began with secondary brine injection to establish initial oil recovery through waterflooding. Once a water breakthrough was observed, with minimal oil production, the WAG injection phase was initiated. Initially, CO_2 was injected at a constant rate of 0.5 ml/min to meet 0.2 pore volumes (PV), followed by a 2-hour soak period. This procedure was repeated until oil production ceased. The soak time allowed CO_2 to interact with the oil, enhancing recovery via mechanisms such as oil swelling, viscosity reduction, and pressure equalization, even in the experimental setup[44]. Previous studies suggest that shorter soak periods are more

Core sample code	BB	B	K
RF (%)	54.48	57.73	49.81

Table 3. Overall RFs for three core samples.
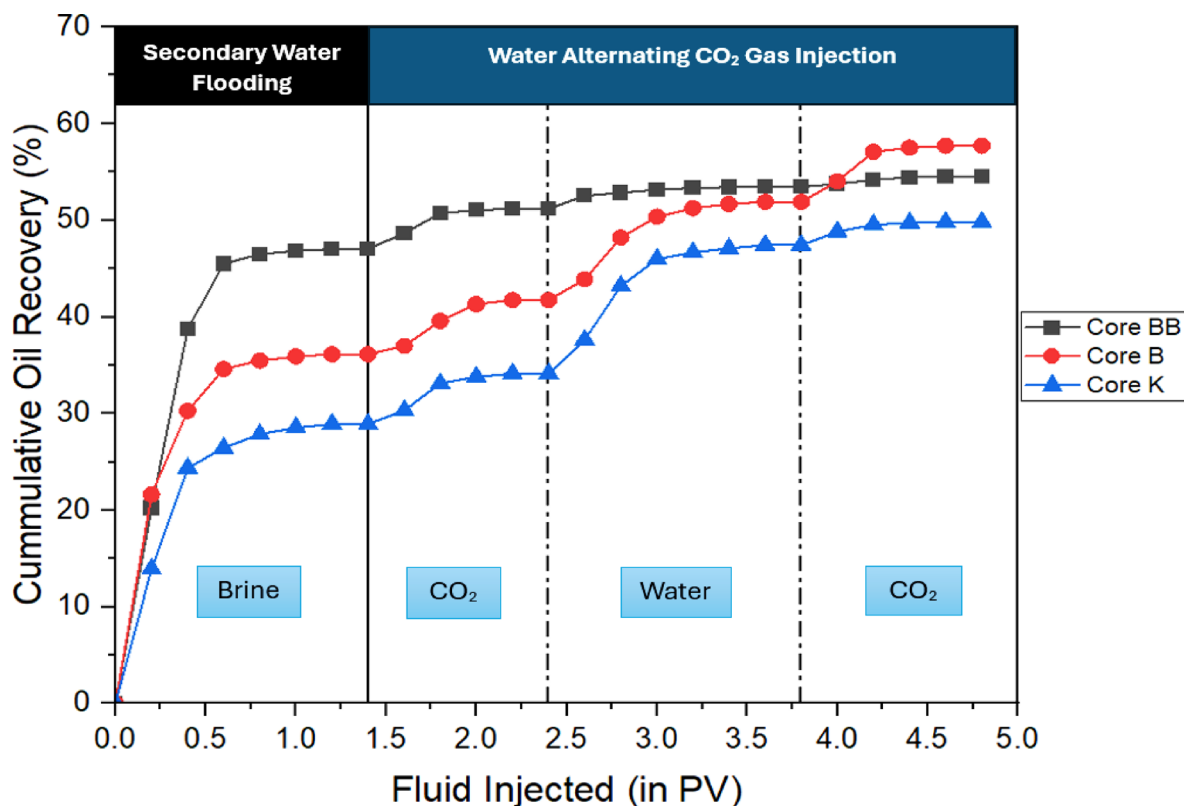
Fig. 6. Cumulative Oil recovery versus fluid injected for all three core samples.

operationally efficient, as prolonged soaking yields diminishing returns in immiscible flooding scenarios due to very limited mass transfer[45].

After the CO_2 injection phase, water was injected at regular intervals until no oil was produced, thus establishing the WAG injection phenomena. CO_2 injection was then resumed following the same procedure until a gas breakthrough was observed at the outlet. Overall, four flooding cycles were conducted for oil recovery. It was found that for all three cases, oil production ceased at equivalent intervals before progressing to the next step. The ultimate recovery factor (RF) obtained from each core sample are shown in Table 3, and Fig. 6 shows the oil recovery under injection sequences. The slight differences in RF among the three cores are primarily due to variations in porosity, permeability, and mineralogical composition. Core B exhibits the highest recovery due to better connectivity and favorable rock-fluid interactions, while Core K shows the lowest due to potential permeability restrictions or mineralogical constraints affecting CO_2 flooding efficiency.

Core BB, which shows the highest recovery during secondary waterflooding, likely has a larger pore throat radius and better pore connectivity, enabling efficient brine displacement and early oil production. However, during WAG, its performance plateaus, possibly due to gas channeling or dominance of macropores, which limits CO_2 sweep efficiency[46]. Core B shows a gradual stepwise increase, suggesting a more heterogeneous pore structure where CO_2 alternation accesses previously unswept zones. In contrast, Core K exhibits the lowest recovery, which is due to tighter pore networks, higher capillary pressure, or stronger oil-wet characteristics, all of which hinder fluid displacement during both water and CO_2 injection[46,47].

Recovery in various phases of flooding
Secondary Brine flooding
In secondary water flooding (Fig. 6), Core BB achieves the highest oil recovery of 47% due to its superior porosity and permeability, which allow the brine to flow more uniformly through interconnected pore networks. The high permeability reduces flow resistance, improving sweep efficiency and enhancing oil displacement. This leads to greater initial recovery as water can easily mobilize oil trapped in larger pore spaces compared to less permeable cores[48]. Moreover, the microscopic mechanisms, such as water-stripping effects and efficient pore-wall interactions, further enhance the oil recovery in high-permeability reservoirs. However, issues like

water channeling may still occur if heterogeneities exist, limiting ultimate recovery. Core B follows with 38% recovery, showing moderate sweep efficiency, while Core K records the lowest recovery at 28%, likely due to lower permeability and capillary trapping effects. Research confirms that reservoirs with high porosity and permeability are better suited for water flooding due to their ability to minimize capillary trapping and improve oil mobilization efficiency[49].

First phase of WAG injection (CO_2 injection)
Figure 7 emphasizes the impact of soak time in oil recovery as well as how permeability affects CO_2 injection efficiency. Due to early gas breakthrough at 5 PV, where CO_2 quickly channels down high-permeability pathways, avoiding oil-rich zones and decreasing sweep efficiency, Core BB, which has the highest permeability, recovers only 4% of the oil. However, because CO_2 distributes more evenly and interacts with the oil for a longer period, Core B, which has intermediate permeability, delays gas breakthrough to 7 PV and achieves the highest recovery (~ 6%). By preventing gas channeling, Core K, which has the lowest permeability, performs better than Core BB with a recovery rate of 5.5%. This enables a longer CO_2-oil interaction and improved sweep efficiency.

The 2-hour soak time between intervals plays a crucial role in improving oil displacement, as it allows CO_2 to diffuse deeper into the pore spaces, enhancing miscibility and oil swelling. Cores with lower permeability, such as K, benefit the most from extended soak time since the slower gas movement ensures more effective oil contact, reducing viscosity and improving recovery[50]. This trend underscores how permeability and soak time dictate CO_2 flood efficiency; higher permeability leads to rapid gas breakthrough and poor sweep, while controlled gas flow and extended soaking in lower-permeability cores enhance displacement efficiency and ultimate recovery.

Second phase of WAG injection (water injection)
Figure 8 shows cumulative oil recovery during the water injection phase following CO_2 injection. Core K, with the lowest permeability, achieves the highest recovery of 13.3% due to better water sweep efficiency and reduced early breakthrough. Core BB, despite its high permeability, shows minimal incremental recovery of only 2.2% increment showing constant production throughout as water channels through high-flow pathways, bypassing residual oil[51–53]. Core B demonstrates a moderate recovery of 10.16% due to balanced permeability, enhancing displacement efficiency.

Third phase of WAG injection (CO_2 injection)
Figure 9 represents cumulative oil recovery during the final CO_2 injection phase of the WAG process, and was done until only CO_2 gas came out with no other extra fluids. Core B achieves the highest recovery factor of 5.83%, which implies that CO_2 interaction, along with water and oil with prerequisite soak time, could assist in removing some portion of residual oil from the core. Core K achieved a slow, gradual increase from starting this
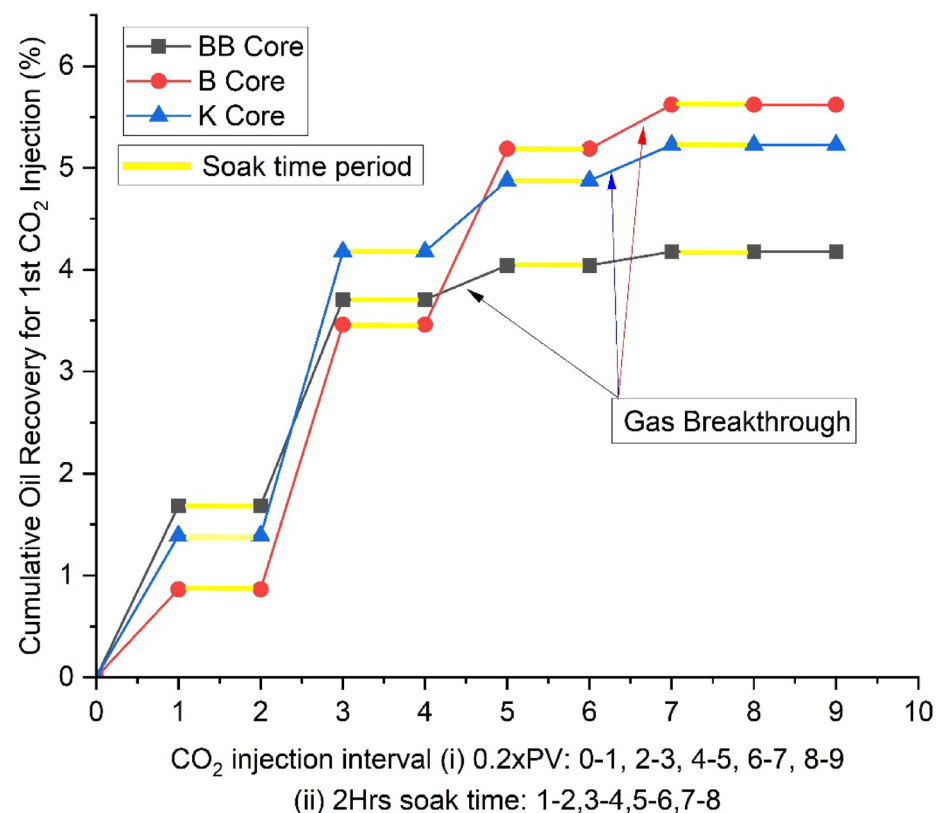

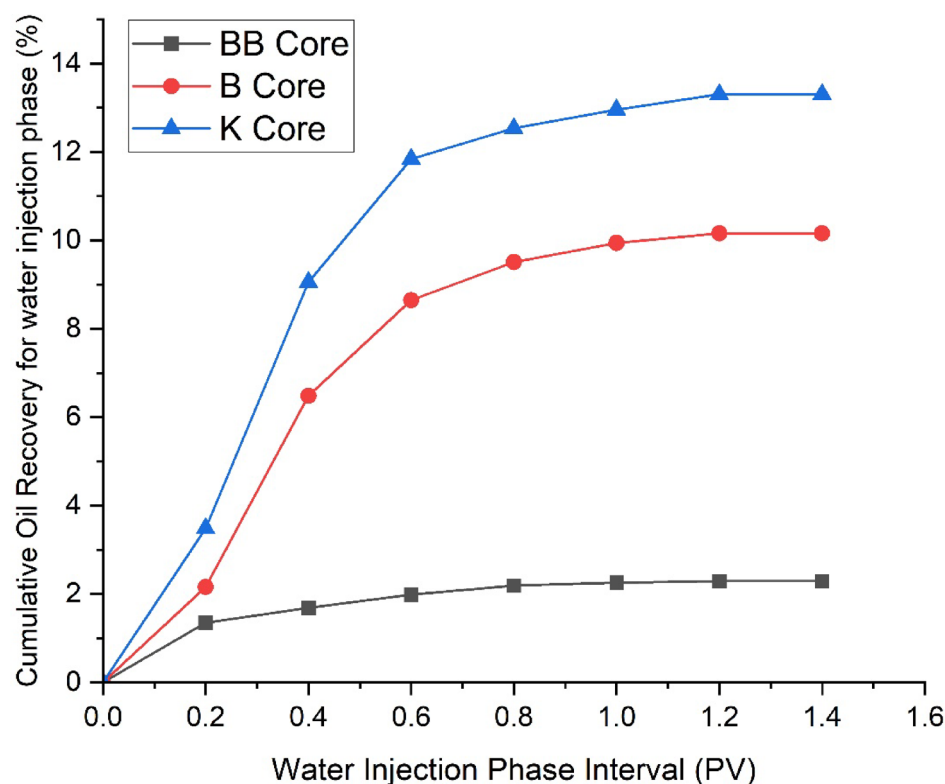**Fig. 7.** Cumulative oil recovery in the initial CO_2 injection phase (WAG).

Fig. 8. Cumulative oil recovery in water injection phase (WAG).

phase and remained constant after 3rd interval of the soak period, with an overall 2.36% having some impact of water[54]. And lastly, the core BB exhibits the least recovery of 1.01%, showing the negligible impact of the sequential injection with CO_2 at last due to faster breakthroughs in previous stages.

Variation in differential pressure during injection phases

The differential pressure exerted within the core flooding processes with a certain sequential pattern has been illustrated in Fig. 10 as it was determined from every pore volume injection. The graph demonstrates the permeability-dependent behavior of the cores. When the pressure difference exceeds a specific threshold of 330 to 350 psi, the pressure difference curves exhibit a cliff-like decline. There are two explanations for this phenomenon: (i) CO_2 dissolves in crude oil, causing a slow decline in pressure difference[55], which is less relevant because it was immiscible flooding; (ii) after the CO_2 breakthrough, the pressure difference rapidly decreases because the gas-phase flow resistance is much lower than the oil-phase flow resistance. When the CO_2 gas reaches a complete breakthrough, the pressure difference is mostly caused by gas flow resistance, resulting in a tiny and steady pressure differential[56]. As water was injected after CO_2 injection, pressure building was initiated which helped prevent gas migration and assisted in pushing some residual oil. Further gas injection also developed some differential pressure ranging from 50 – 10 psi which also helped for more recovery. From the second stage of WAG, it was found that sample BB did not have much impact on flooding as the complete breakthrough of water and gas has taken place.

The three graphs in Fig. 11 prove that Sample BB exhibits the highest oil recovery efficiency till secondary brine flooding only due to its high permeability and minimal flow resistance but showed fewer recovery trends in WAG stages. Both B and K core samples have better recovery trends in WAG stages which can be seen by R-squared values of linearity trendline also highlighting slope and intercept with sample BB having the lowest of 55% and the other two in-between the range of 85–95% that illustrates better sweep efficiency BB sample shows almost linear cumulative recovery from 80 psi, but B and K samples have a gradual increase in both recovery and pressure, which proves the impact of WAG in creating better pressure difference for oil recovery. The amount of constant soak time that has been implemented during the sequential injection for each core has little impact on the recovery for samples B and K which implies even if immiscible, CO_2 dissolution has taken place in some amount during flooding[57].

Comparative study

Table 4 presents a comparison of various CO_2 flooding techniques used for oil recovery, along with the corresponding study results. The experimental-scale comparison indicates that CO_2 flooding methods incorporating WAG consistently outperform other techniques in oil recovery. In this paper, water-alternating
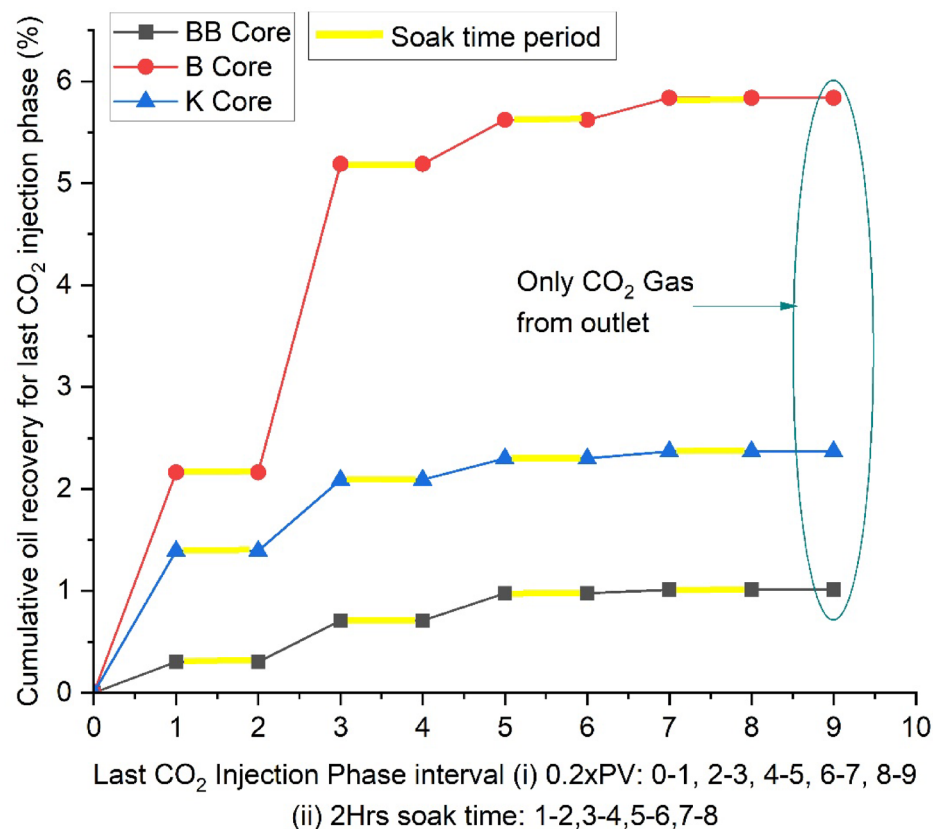
Fig. 9. Cumulative oil recovery in the last CO_2 injection phase (WAG).
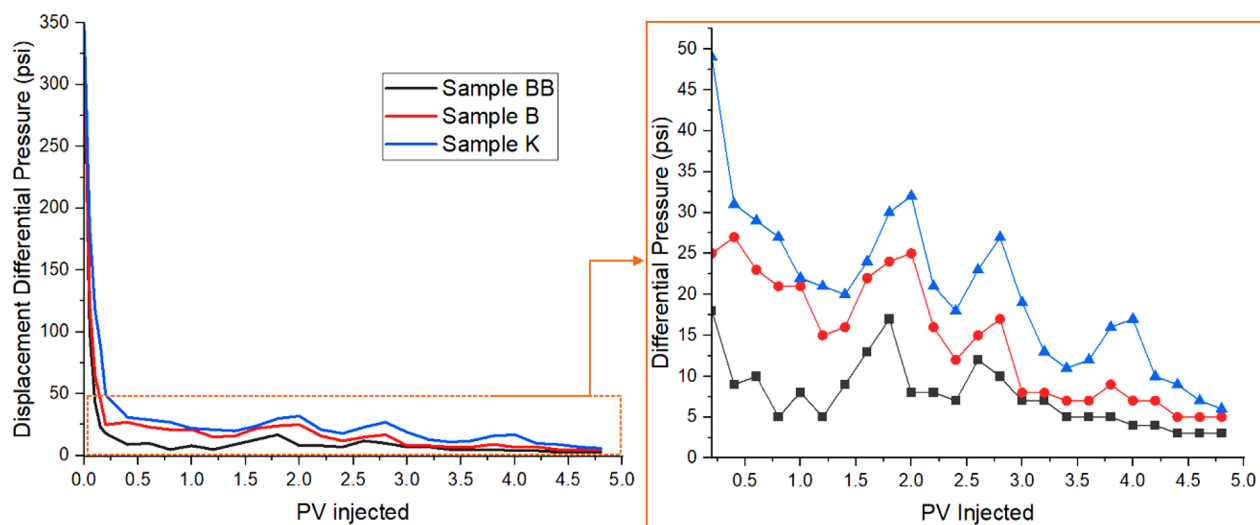

Fig. 10. Variations in the pressure difference with injected pore volume during flooding.

CO_2 gas injection achieved optimal OOIP in resemble cores, further highlighting the importance of sequential flooding cycles combined with optimal soak times.

Limitations of the study and way forward

The present study did not include pore size distribution analysis, limiting the understanding of pore-scale fluid behavior and heterogeneity impact on CO_2 displacement. Advanced imaging techniques like SEM (Scanning Electron Microscopy) and pore typing via NMR (Nuclear Magnetic Resonace) were not employed, which could have provided valuable insights into pore connectivity, wettability, and capillary forces. Additionally, the
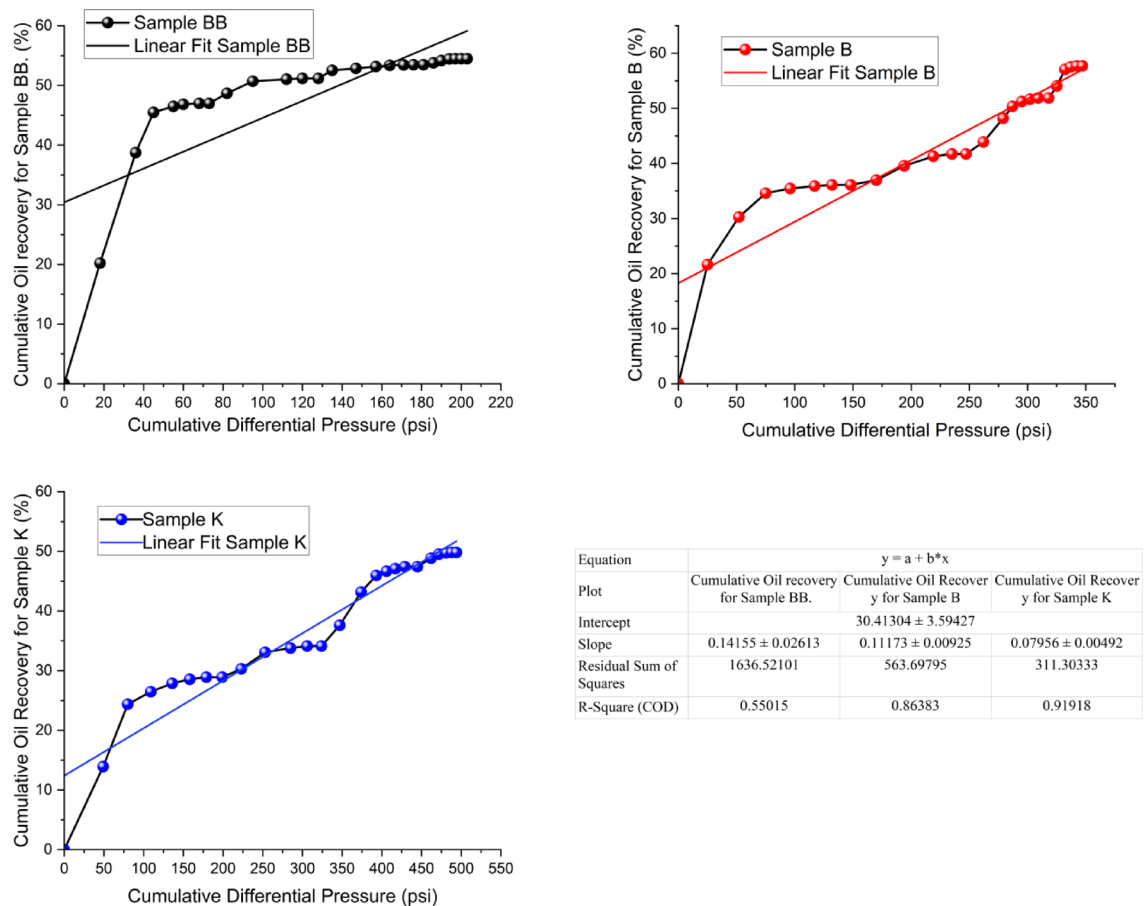
Fig. 11. Variations of cumulative differential pressure for cumulative oil recovery for each core sample.

The equation table from the figure:

Equation	y = a + b*x		
Plot	Cumulative Oil recovery for Sample BB.	Cumulative Oil Recovery for Sample B	Cumulative Oil Recovery for Sample K
Intercept		30.41304 ± 3.59427	
Slope	0.14155 ± 0.02613	0.11173 ± 0.00925	0.07956 ± 0.00492
Residual Sum of Squares	1636.52101	563.69795	311.30333
R-Square (COD)	0.55015	0.86383	0.91918

Literature	Core Samples Used	Porosity (%)/Permeability (mD)	CO₂ Flooding Method	Temperature, Pressure, Flow Rate/Time	No. of Flooding Cycles	Ultimate Oil Recovery (Best Observed)
58	Tight sandstone cores from Chang 6 reservoir, China	Porosity: ~9%, Permeability: 0.1–0.2 mD	Continuous CO_2 injection with pressure cycling	45 °C, Pressure: 30 MPa, Flow rate: ~0.5 ml/min	3 cycles	38.96% OOIP under optimal conditions
59	Tight sandstone core	Porosity: 8–12%, Permeability: <1 mD	Cyclic CO_2 injection with water-alternating-gas (WAG)	60 °C, 3000 psi, Flow rate: 0.5 ml/min	4 Cycles	48% OOIP (best achieved during cyclic injection)
60	Berea Sandstone Core	Porosity: ~22%, Permeability: ~750 mD	High-pressure cyclic CO_2 injection and WAG injection	50 °C, 12 MPa, Flow rate: ~0.5 ml/min	5 Cycles	68% OOIP in the final cycle gives optimal soak time.
61	N formation in M oilfield	Porosity: ~14%, Permeability: ~6.5 mD	Huff and Puff's process of CO_2, ethyl ether until there is no oil produced	60 °C, 1.5–2.0 MPa, Flow Time: 0–308 min	3 Cycles	Nearly 25% by the CO_2 huff and puff process in 3 rounds (neglecting OOIP)
62	Fractured sandstone cores	Porosity: ~12%, Permeability: ~1 mD	CO_2 foam flooding	70 °C, 10 MPa (100 bar), Flow rate: ~1 cc/min	3 Cycles	65% OOIP in the fractured core under foam EOR
63	Reservoir sandstone from Kazakhstan	Porosity: 15–18%, Permeability: 10–50 mD	CO_2 EOR	70 °C, 2000 psi, Flow rate: 0.2 ml/min	3 Cycles	55% OOIP (best observed at high-pressure injection)
64	Multi-Layered Heterogenous Reservoir	Core of 2800 mD/780 mD, 360 mD	Microgel alternate CO_2 flooding	-	-	Based on WAG is 12.4%
65	Cylindrical Berea cores	Gas permeabilities are about 5 mD, 10 mD, and 20 mD	Polymer-assisted CO_2 flooding using Temperature resistance polymer surfactant slug	Maximum of 10 MPa	-	Based on CO_2 flooding is 32.93%; based on water-assisted CO_2 flooding is 8.21%
66	Berea core samples	Porosity: ~ 20% Permeability: ~31 mD	Polymer-assisted CO_2 flooding using Polyfluoroacrylate	3000 psi, Flow rate: 0.25 ml/min or 2.5 ml/min	-	Based on CO_2 flooding is 16%
Present Study	X-field, Cambay Basin sandstone cores	Porosity: ~17–28%; Permeability: ~100–300 mD	Water Alternating CO_2 Gas Injection	80 °C, Maximum 350–400 psi, 0.5 ml/min	4 cycles	Overall recovery varies from 49 ~ 55%

Table 4. Comparison of oil recovery from various experimental scale CO_2 flooding:.

absence of slim tube experiments means that MMP was not determined accurately i.e. only by using correlations, preventing confirmation of miscibility conditions. The lack of multiple injection scenarios and simulation-based validation also restricts the generalization of laboratory findings to field applications.

Future work should include detailed pore size distribution analysis through MICP (Mercury Injection Capillary Pressure), SEM, and NMR to correlate pore geometry before and after the injection process with oil recovery trends under CO_2-WAG injection. Comparative NMR and SEM studies can help classify pore types, wettability states, and movable fluid volumes. Slim tube experiments must be conducted to accurately determine the MMP for X-field crude oil, allowing optimized miscible or near-miscible CO_2 flooding. Integration with simulation models and exploring hybrid WAG methods (e.g., foam or surfactant-assisted) could further enhance displacement efficiency and CO_2 storage potential.

Conclusions

The effect of water alternating CO_2 gas injection in variable petrophysical cores and the influence of injection patterns including soak time, pressure build and flow rate on the flooding process were systematically studied in the present study. Based on the present work, the following conclusions may be drawn:

- FTIR analysis confirmed a strong presence of long-chain aliphatic hydrocarbons, with CH_2 stretching peaks at 2925 cm^{-1} and 2853 cm^{-1}, and minor aromatic compounds identified by weak peaks at 813 cm^{-1} and 743 cm^{-1}, suggesting a molecular structure conducive to CO_2-induced viscosity reduction and oil swelling. XRD analysis of sandstone cores revealed quartz as the dominant mineral (> 70%), with feldspar (~ 15%) and a negligence amount of kaolinite feasible for CO_2 interaction in some amount while flooding.
- The recovery trends highlight the impact of sequential water-alternating CO_2 injection on oil displacement efficiency. In secondary brine injection, Core BB achieved the highest initial recovery (47%) due to better fluid flow, while Core B (38%) and Core K (28%) showed lower recovery due to capillary trapping. During the first CO_2-WAG phase, Core B had the highest incremental recovery (6%), followed by Core K (5.5%), while Core BB (4%) suffered from early gas channeling. Water injection further improved Core K's recovery (13.3%) due to better sweep efficiency, with Core B at (10.16%) and Core BB at (2.2%). The final CO_2 injection phase yielded diminishing returns, with Core B gaining (5.83%), Core K (2.36%), and Core BB only (1.01%) due to gas breakthrough. Overall, moderate-permeability cores balanced CO_2-oil interaction and delayed breakthrough, achieving the highest recovery, while highly permeable cores faced early bypassing and lower long-term efficiency.
- The differential pressure trends highlight recovery efficiency variations among cores. In Core BB, early CO_2 breakthrough caused a sharp pressure drop (330–350 psi to 10–50 psi) and minimal WAG impact (R^2 = 55%). In contrast, Cores B and K maintained better pressure control, achieving R^2 values of 85–95%, indicating improved sweep efficiency. While soak time had little effect on BB, it contributed to gradual oil displacement in B and K, suggesting partial CO_2 dissolution. These results confirm that WAG injection is more effective in delaying gas breakthroughs and enhancing oil recovery in select cores.

Data availability

The datasets generated and analyzed during the current study are not publicly available due to institutional restrictions but are available from the corresponding author upon reasonable request.

References

1. Zafar, S. A. et al. Mechanisms and molecular approaches for heat tolerance in rice (Oryza sativa L.) under climate change scenario. *J. Integr. Agric.* **17**, 726–738 (2018).
2. Kabir, M. et al. Climate change due to increasing concentration of carbon dioxide and its impacts on environment in 21st century; a mini review. *J. King Saud Univ. Sci.* **35**, 102693 (2023).
3. Li, L. et al. Influence of heterogeneity and fracture conductivity on supercritical CO2Miscible flooding enhancing oil recovery and gas channeling in tight oil reservoirs. *Energy Fuels.* **36**, 8199–8209 (2022).
4. Afzali, S., Rezaei, N. & Zendehboudi, S. A comprehensive review on enhanced oil recovery by water alternating gas (WAG) injection. *Fuel* **227**, 218–246 (2018).
5. Bello, A. et al. Numerical study of the mechanisms of nano-assisted foam flooding in porous media as an alternative to gas flooding. *Heliyon* **10**, (2024).
6. Fang, P. et al. Chemical-Assisted CO2 Water-Alternating-Gas injection for enhanced sweep efficiency in CO2-EOR. *Molecules* **29**, (2024).
7. Ghedan, S. Global Laboratory Experience of CO2-EOR Flooding. Society of Petroleum Engineers - SPE/EAGE Reservoir Characterization and Simulation Conference 2009 - Overcoming Modeling Challenges to Optimize Recovery 2, 883–897 (2009).
8. Wang, Z. et al. Unveiling nanoscale fluid miscible behaviors with nanofluidic slim-tube. *Energy Environ. Sci.* **17**, 9635–9651 (2024).
9. Chen, X. et al. Enhancing oil recovery in low permeability reservoirs through CO2 miscible flooding: mechanisms and dynamics. *ACS Omega.* https://doi.org/10.1021/ACSOMEGA.4C06509/ASSET (2024).
10. Yin, M. CO_2 miscible flooding application and screening criteria. Masters Theses (2015).
11. Emami-Meybodi, H. et al. Cyclic gas injection in Low-Permeability oil reservoirs: progress in modeling and experiments. *SPE J.* **29**, 6217–6250 (2024).
12. Bijeljic, B., Muggeridge, A. H. & Blunt, M. J. Multicomponent mass transfer across water films during hydrocarbon gas injection. *Chem. Eng. Sci.* **58**, 2377–2388 (2003).
13. Cui, M., Wang, R., Lv, C. & Tang, Y. Research on microscopic oil displacement mechanism of CO2 EOR in extra-high water cut reservoirs. *J. Pet. Sci. Eng.* **154**, 315–321 (2017).
14. Shen, H. et al. CO2-responsive agent for restraining gas channeling during CO2 flooding in low permeability reservoirs. *Fuel* **292**, 120306 (2021).

15. Rawat, A. et al. Simulation-driven sensitivity analysis and optimization of critical parameters for maximizing CO2-EOR efficiency. *Petroleum Res.* https://doi.org/10.1016/J.PTLRS.2025.02.007 (2025).

16. Kamali, F., Hussain, F. & Cinar, Y. A. Laboratory and Numerical-Simulation study of Co-Optimizing CO2 storage and CO2 enhanced oil recovery. *SPE J.* **20**, 1227–1237 (2015).

17. Kulkarni, M. M. & Rao, D. N. Experimental investigation of miscible and immiscible Water-Alternating-Gas (WAG) process performance. *J. Pet. Sci. Eng.* **48**, 1–20 (2005).

18. Rezaei, M., Shadizadeh, S. R., Vosoughi, M. & Kharrat, R. An experimental investigation of sequential CO2 and N2 gas injection as a new EOR method. *Energy Sour. Part A Recover. Utilization Environ. Eff.* **36**, 1938–1948 (2014).

19. Seyyedsar, S. M., Farzaneh, S. A. & Sohrabi, M. Enhanced heavy oil recovery by intermittent CO2 injection. *Proc. - SPE Annual Tech. Conf. Exhib.* **2015-January**, 6177–6193 (2015).

20. Nasser, S. M. M., Bera, A. & Ramalingam, V. Comparative studies on numerical sensitivity of different scenarios of enhanced oil recovery by water-alternating-gas (CO2) injection. *Petroleum Res.* **8**, 505–513 (2023).

21. Ratanpara, A. et al. Hybrid Huff-n-Puff process for enhanced oil recovery: integration of surfactant flooding with CO2 oil swelling. *Appl. Sci. (Switzerland).* **14**, 12078 (2024).

22. LIU, X. et al. Oil production characteristics and CO2 storage mechanisms of CO2 flooding in ultra-low permeability sandstone oil reservoirs. *Pet. Explor. Dev.* **52**, 196–207 (2025).

23. Majidaie, S., Onur, M. & Tan, I. M. An experimental and numerical study of chemically enhanced water alternating gas injection. *Pet. Sci.* **12**, 470–482 (2015).

24. Samba, M. A. & Elsharafi, M. O. Literature review of water alternation gas injection. *J. Earth Energy Eng.* **7**, 33–45 (2018).

25. Qays, H. et al. Fuel parameter analysis from kerosene blended with biodiesel and diesel fuel. *IOP Conf. Ser. Earth Environ. Sci.* **1104**, 012036 (2022).

26. Nadkarni, R. Guide to ASTM test methods for the analysis of petroleum products and lubricants, 2nd edition. *Guide ASTM Test. Methods Anal. Petroleum Prod. Lubricants 2ND Ed.* https://doi.org/10.1520/MNL44-2ND-EB (2007).

27. Mmata, B., Ajienka, J., Onyekonwu, M. & Chukwu, G. Determination of wax precipitation tendency using Sara analysis. *Soc. Petroleum Eng. - Nigeria Annual Int. Conf. Exhib.* **2017**, 323–331. https://doi.org/10.2118/189130-MS (2017).

28. Waner, N. S., Alston, A., Podkulski, D. E. & Verhappen, I. Physical properties analyzers—ASTM methods. Instrument engineers' handbook: process measurement and analysis. *Fourth Ed.* 1589–1605. https://doi.org/10.1201/9781315137469-48/PHYSICAL-PROPERTIES-ANALYZERS (2003).

29. Ahmadi, Y. et al. Comprehensive Water-Alternating-Gas (WAG) injection study to evaluate the most effective method based on heavy oil recovery and asphaltene precipitation tests. *J. Pet. Sci. Eng.* **133**, 123–129 (2015).

30. Shalygin, A. S., Kozhevnikov, I. V., Morozov, E. V. & Martyanov, O. N. Features of wax appearance temperature determination of waxy crude oil using attenuated total reflection fourier transform infrared spectroscopy under ambient and high pressure. *Appl. Spectrosc.* **78**, 277–288 (2024).

31. Nisar, J. et al. Enhanced biodiesel production from Jatropha oil using calcined waste animal bones as catalyst. *Renew. Energy.* **101**, 111–119 (2017).

32. Banerjee, S., Kumar, S., Mandal, A. & Naiya, T. K. Design of novel chemical solvent for treatment of waxy crude. *Int. J. Oil Gas Coal Technol.* **15**, 363–379 (2017).

33. Tariq, M. et al. FT-IR, NMR (1H and 13 C) and GC/MS studies of fatty acid Methyl esters in biodiesel from rocket seed oil. *Fuel Process. Technol.* **92**, 336–341 (2011).

34. Safar, M., Bertrand, D., Robert, P., Devaux, M. F. & Genot, C. Characterization of edible oils, butters and margarines by fourier transform infrared spectroscopy with attenuated total reflectance. *J. Am. Oil Chem. Soc.* **71**, 371–377 (1994).

35. Haghtalab, A., Mohammadi, M. & Fakhroueian, Z. Absorption and solubility measurement of CO2 in water-based ZnO and SiO2 nanofluids. *Fluid Phase Equilib.* **392**, 33–42 (2015).

36. Ngo, I., Sasaki, K., Ma, L., Nguele, R. & Sugai, Y. Enhancing surfactant desorption through low salinity water post-flush during enhanced oil recovery. *Oil Gas Sci. Technol.* **76**, (2021).

37. Ariketi, R., Bhui, U. K., Chandra, S. & Biswal, S. Brittleness modeling of Cambay shale formation for shale gas exploration: a study from Ankleshwar area, Cambay basin, India. *J. Pet. Explor. Prod. Technol.* **7**, 911–923 (2017).

38. Ray, D. et al. Formulation of Polymer-Augmented Surfactant-Based oil-Water microemulsions for application in enhanced oil recovery. *ACS Omega.* https://doi.org/10.1021/ACSOMEGA.4C09829/ASSET (2024).

39. Yellig, W. F. & Metcalfe, R. S. Determination and prediction of CO2 minimum miscibility pressures (includes associated paper 8876). *J. Petrol. Technol.* **32**, 160–168 (1980).

40. Pratap, M., Roy, R. P., Gupta, R. K. & Singh, D. Field implementation of polymer EOR Technique - A successful experiment in India. *SPE Annual Tech. Conf. Exhib.* **5**, 8. https://doi.org/10.2118/38872-MS (1997).

41. Gorain, S. & Thakur, P. Attribute based inversion a tool for reservoir characterization: a case study-Kalol field, Cambay basin, India. *Acta Geod. Geoph.* **50**, 321–338 (2015).

42. Holm, L. R. W. & Josendal, V. A. Effect of oil composition on miscible-type displacement by carbon dioxide. SPEJ, Soc. Pet. Eng. J.; (United States) 22:1, 87–98 (1982).

43. Leung, L. C. Numerical evaluation of the effect of simultaneous steam and carbon dioxide injection on the recovery of heavy oil. *J. Petrol. Technol.* **35**, 1591–1599 (1983).

44. Li, S., Zhang, K., Jia, N. & Liu, L. Evaluation of four CO2 injection schemes for unlocking oils from low-permeability formations under immiscible conditions. *Fuel* **234**, 814–823 (2018).

45. Pi, Y. et al. Investigation of the influence of formation water on the efficiency of CO2 miscible flooding at the core scale. *Processes 2023.* **11** (Page 2954 11), 2954 (2023).

46. Iglauer, S. CO2-Water-Rock wettability: variability, influencing factors, and implications for CO2 geostorage. *Acc. Chem. Res.* **50**, 1134–1142 (2017).

47. Olabode, O. A., Orodu, O. D., Isehunwa, S. O., Mamudu, A. & Rotimi, O. J. Effect of foam and WAG (water alternating gas) injection on performance of thin oil rim reservoirs. *J. Pet. Sci. Eng.* **171**, 1443–1454 (2018).

48. Li, Y. et al. Experimental Study on Microscopic Water Flooding Mechanism of High-Porosity, High-Permeability, Medium-High-Viscosity Oil Reservoir. Energies 2023, Vol. 16, Page 6101 16, 6101 (2023).

49. Zhou, W., Yin, D. & Zhou, Y. The seepage mechanism of Micro remaining oil during Cyclic waterflooding in Low-permeability reservoir. *J. Phys. Conf. Ser.* **2584**, (2023).

50. Huang, E. T. S. & Holm, L. W. Effect of WAG injection and rock wettability on oil recovery during CO2 flooding. *SPE. Reserv. Eng.* **3**, 119–129 (1988).

51. Li, D., Saraji, S., Jiao, Z. & Zhang, Y. CO2 injection strategies for enhanced oil recovery and geological sequestration in a tight reservoir: an experimental study. *Fuel* **284**, (2021).

52. Alkhazmi, B., Farzaneh, A., Sohrabi, S. & Sisson, A. M. An Experimental Investigation of WAG Injection Performance under Near-Miscible Conditions in Carbonate Rock and Comparison with Sandstone. SPE Western Regional Meeting Proceedings 2018-April, SPE-190053-MS (2018).

53. Al-Menhali, A. S. & Krevor, S. Capillary trapping of CO2 in oil reservoirs: observations in a Mixed-Wet carbonate rock. *Environ. Sci. Technol.* **50**, 2727–2734 (2016).

54. Afzali, S., Ghamartale, A., Rezaei, N. & Zendehboudi, S. Mathematical modeling and simulation of water-alternating-gas (WAG) process by incorporating capillary pressure and hysteresis effects. *Fuel* **263**, (2020).

55. Zhou, X. et al. Determining CO2 diffusion coefficient in heavy oil in bulk phase and in porous media using experimental and mathematical modeling methods. *Fuel* **263**, 116205 (2020).
56. Zhu, W. et al. The effect of injection pressure on the microscopic migration characteristics by CO2 flooding in heavy oil reservoirs. *Energy Sources Part. A: Recovery Utilization Environ. Eff.* **44**, 1459–1467 (2022).
57. Al-Obaidi, D. A. & Al-Jawad, M. S. Immiscible CO2-Assisted gravity drainage process for enhancing oil recovery in bottom water drive reservoir. *Association Arab. Universities J. Eng. Sci.* **27**, 60–66 (2020).
58. Zhou, X. et al. Performance evaluation of CO2 flooding process in tight oil reservoir via experimental and numerical simulation studies. *Fuel* **236**, 730–746 (2019).
59. Li, D. et al. Determination of minimum miscibility pressure of CO2–Oil system: A molecular dynamics study. *Molecules 2021*. **26**, 4983 (2021).
60. Wang, L., Zhao, Q. & Li, Z. Experimental investigation of carbon dioxide flooding in heavy oil reservoirs for enhanced oil recovery. *Energy Rep.* **8**, 10754–10761 (2022).
61. Kang, H., Gao, J. & Hui, G. Laboratory evaluation of CO2 flooding: A strategic technology for sustainable development of oil companies. *Strategic Plann. Energy Environ.* **42**, 21–36 (2023).
62. Zhu, D. et al. Experimental investigation of CO2 foam flooding-enhanced oil recovery in fractured low-permeability reservoirs: Core-scale to pore-scale. *Fuel* **362**, 130792 (2024).
63. Shabdirova, A. et al. Core flooding experiments on the impact of CO2-EOR on the petrophysical properties and oil recovery parameters of reservoir sandstones in Kazakhstan. *Geosci. 2024*. **14** (Page 185 14), 185 (2024).
64. Liu, Z. et al. Conformance control by a microgel in a multi-layered heterogeneous reservoir during CO2 enhanced oil recovery process. *Chin. J. Chem. Eng.* **43**, 324–334 (2022).
65. Chen, X. et al. Investigation of Polymer-Assisted CO2 flooding to enhance oil recovery in Low-Permeability reservoirs. *Polym. 2023*. **15**, 3886 (2023).
66. Zaberi, H. A. et al. An experimental feasibility study on the use of CO2-soluble polyfluoroacrylates for CO2 mobility and conformance control applications. *J. Pet. Sci. Eng.* **184**, (2020).

Acknowledgements

Author contributions

A.R. contributed to the writing of the original draft, experimental development studies, methodology, investigation, formal analysis, data curation, and conceptualization. B.K. was responsible for experimental development studies, resources, investigation, formal analysis, and data curation. A.K.S. contributed to writing, specifically in review and editing. P.N. and B.M. was involved in the investigation. A.B. participated in writing through review and editing, as well as validation. N.B. and B.D. played a key role in writing (review and editing), supervision, software development, resource management, project administration, methodology, investigation, formal analysis, data curation, and conceptualization. Finally, A.S. provided supervision.

Declarations

Competing interests

The authors declare no competing interests.

Additional information

Correspondence and requests for materials should be addressed to N.B.

Reprints and permissions information is available at www.nature.com/reprints.

Publisher's note Springer Nature remains neutral with regard to jurisdictional claims in published maps and institutional affiliations.